



Neuroactive Peptide Nanofibers for Regeneration of Spinal Cord after Injury

Melike Sever-Bahcekapili, Canelif Yilmaz, Altan Demirel, Mustafa Cemil Kilinc, Ihsan Dogan, Yusuf Sukru Caglar,* Mustafa O. Guler,* and Ayse B. Tekinay*

The highly complex nature of spinal cord injuries (SCIs) requires design of novel biomaterials that can stimulate cellular regeneration and functional recovery. Promising SCI treatments use biomaterial scaffolds, which provide bioactive cues to the cells in order to trigger neural regeneration in the spinal cord. In this work, the use of peptide nanofibers is demonstrated, presenting protein binding and cellular adhesion epitopes in a rat model of SCI. The self-assembling peptide molecules are designed to form nanofibers, which display heparan sulfate mimetic and laminin mimetic epitopes to the cells in the spinal cord. These neuroactive nanofibers are found to support adhesion and viability of dorsal root ganglion neurons as well as neurite outgrowth *in vitro* and enhance tissue integrity after 6 weeks of injury *in vivo*. Treatment with the peptide nanofiber scaffolds also show significant behavioral improvement. These results demonstrate that it is possible to facilitate regeneration especially in the white matter of the spinal cord, which is usually damaged during the accidents using bioactive 3D nanostructures displaying high densities of laminin and heparan sulfate-mimetic epitopes on their surfaces.

and endothelial cells create an inhibitory environment for neurons by inducing the formation of a glial scar, which acts as both mechanical and chemical barrier preventing the regeneration of the axons. In addition, the blood-spinal cord barrier encourages the permanence of glial scars through slowing down the infiltration of macrophages, which are required for cleaning of the debris.^[3] Therefore, current clinical treatments are generally limited to providing pain relief and the prevention of secondary injuries through administration of anti-inflammatory drugs.^[4] Until now, many potential strategies have been studied including transplantation of fetal spinal cord tissue,^[5] Schwann cells,^[6] peripheral nerves,^[7] embryonic stem cells,^[8] bone marrow stromal cells,^[9] neural stem cells,^[10] and genetically modified cells.^[11,12] Due to lack of adequate fetal tissue sources and autol-

ogous nerve grafts, the use of cells cultured *in vitro* can be a more viable solution for transplantation. The cellular therapy approach requires a bioactive filling for the defect site for better tissue regeneration.

Urgent need for the recovery of damaged tissues has encouraged the development of new scaffolds for the treatment of SCI. Naturally derived scaffolds such as collagen and gelatin or synthetic polymers including poly lactic acid, and poly lactic-co-glycolic acid^[13,14] are used as scaffold biomaterials. However,

1. Introduction

Traumatic injuries in the spinal cord cause loss of neural tissue, which is characterized by partial or complete loss of function in the nervous system.^[1,2] For functional recovery after spinal cord injury (SCI), regeneration of the damaged axons across the site of injury is required. The progress of treatments for SCIs is complicated because of a highly complex inhibitory environment of the injury site. The native fibroblasts, neuroglia,

Dr. M. Sever-Bahcekapili, Dr. A. B. Tekinay
Institute of Materials Science and Nanotechnology
National Nanotechnology Research Center (UNAM)
Bilkent University
Ankara 06800, Turkey
E-mail: atekinay@bilkent.edu.tr
C. Yilmaz, Dr. A. B. Tekinay
Neuroscience Graduate Program
Bilkent University
Ankara 06800, Turkey
Dr. A. Demirel
Department of Neurosurgery
Aksaray State Hospital
Aksaray 68200, Turkey

Dr. M. C. Kilinc, Dr. I. Dogan, Dr. Y. S. Caglar
Faculty of Medicine, Department of Neurosurgery
Ankara University
Ankara 06100, Turkey
E-mail: sukrucaglar983@gmail.com
Dr. M. O. Guler
The Pritzker School of Molecular Engineering
The University of Chicago
Chicago, IL 60637, USA
E-mail: mguler@uchicago.edu
Dr. A. B. Tekinay
Eryigit Research and Development Center
Ankara 06380, Turkey

The ORCID identification number(s) for the author(s) of this article can be found under <https://doi.org/10.1002/mabi.202000234>.

DOI: 10.1002/mabi.202000234

naturally derived scaffolds may give rise to introduction of pathogens^[15] while synthetic polymers have limitations in migration and growth of axons in addition to degradation and biocompatibility problems.^[16,17]

Recently, self-assembled peptide amphiphile (PA) nanofibers have demonstrated promising results for in vitro neural differentiation and in vivo neural regeneration,^[18–22] demonstrating the possibility of the use of these materials for the effective treatment of central nervous system (CNS) injuries. PAs are a class of molecules that have great potential to mimic the regulatory characteristics of natural environment of the cells for biological studies as well as therapeutic applications. They are composed of four different regions which are hydrophobic tail, β -sheet forming unit, charged groups and bioactive epitopes. These molecules can self-assemble into nanostructures, predominantly nanofibers, since amphiphilic nature of the PA monomers leads to the assembly of these monomers into nanofibers under physiological conditions. The assembled nanofibers are composed of a hydrophobic core and a hydrophilic shell.^[23] This type of nanostructures displays high bioactivity due to the presence of bio-active epitopes introduced on hydrophilic shell while the non-bioactive hydrophobic alkyl tail constitutes the hydrophobic core. β -sheet forming unit and charged groups are for intermolecular hydrogen bond formation and for water solubility and pH-dependent design of the nanofibers, respectively.^[24] Hydrophobic interactions between alkyl tails as well as β -sheet formation between the PA molecules induce their self-assembly into nanofibers in aqueous environment. In addition, the self-assembled PA nanofibers provide suitable platforms to mimic the natural extracellular matrix (ECM) through incorporation of bioactive signals to the nanofiber system instead of use of the bulk proteins.^[24] The peptide sequence Ile-Lys-Val-Ala-Val (IKVAV), which is a cell-binding domain of laminin, was previously discovered and found to induce neurite extension.^[25] Laminins are fundamental ECM proteins found in the basal lamina, and interact with the integrin receptors on the cells, thereby affecting biological activities such as adhesion and differentiation.^[26] These proteins are also important for the nervous tissue through functioning in the axonal growth and myelination.^[27] Besides integrin receptors, laminin also interacts with heparan sulfate proteoglycans, which in turn induces neurite outgrowth.^[28] Heparan sulfates are highly sulfated glycosaminoglycans which interact with growth factors and increase their local concentrations.^[29] Due to the fundamental roles of laminin and heparan sulfates in the ECM, using epitopes, which mimic their function, provides an important therapeutic approach for nerve regeneration. Although these epitopes have previously been used alone or in combination with each other for other biomedical purposes,^[18,20–22,30] the cooperative effect of laminin and heparan sulfates on SCI has not been studied before. Here, we investigated therapeutic potential of the heparan sulfate and laminin mimetic peptide nanofibers on hemisection SCIs in vivo and their effect on dorsal root ganglion (DRG) neurons in vitro. The bioactive peptide nanofibers were found to support the adhesion, viability and neurite extension of isolated DRG neurons in cell culture. In animal experiments, 6 weeks following treatment of the rat animal models with bioactive

peptide nanofibers, rats with hemisection SCI at the level of T9 or T10 displayed significant behavioral improvement verified with the Basso, Beattie, and Bresnahan (BBB) scale. Histological assessment also showed that bioactive peptide hydrogel injection to the injury site at the spinal cord provided improved tissue integrity by reducing the progressive cell loss, which makes this bioactive system a promising new therapeutic approach to inhibit glial scar formation and to facilitate regeneration after SCIs.

2. Results and Discussion

2.1. Design and Characterization of Peptide Nanofibers

Four different peptide molecules were synthesized for using in both in vitro and in vivo studies. All peptide molecules had a hydrophobic alkyl tail, a lauric acid, and a β -sheet forming peptide sequence, VVAG. Lauryl-VVAGIKVAV-Amide (LN-PA) was designed to mimic the bioactivity of laminin and Lauryl-VVAGEGDK(p-benzosulfonate)S-Amide (GAG-PA) was designed to mimic heparan sulfates with its sulfonate, hydroxyl, and carboxylic acid groups (Figure 1). Positively charged PA molecules were mixed with negatively charged PA molecules in order to induce charge neutralization and trigger gel formation. Also, positively and negatively charged molecules in bioactive group carry different bioactive signals to introduce dual signal in one system. LN-PA/GAG-PA nanofiber scaffolds displayed two bioactive epitopes at the same time to mimic the function of both laminin and heparan sulfate. The other two PA molecules used in this study were Lauryl-VVAGEE (EE-PA) and Lauryl-VVAGKK-Amide (KK-PA) which did not bear any bioactive sequences (Figure 1) but could still form nanofibers in a manner similar to LN-PA/GAG-PA. KK-PA/EE-PA nanofibers were used as an epitope-free control group. The PA molecules were synthesized by solid phase peptide synthesis, purified with preparative high-performance liquid chromatography (HPLC) and characterized by liquid chromatography-mass spectrometry (LC-MS). Scanning Electron Microscopy (SEM) imaging revealed that all peptide nanofibers displayed morphological similarity to natural ECM that surrounds the cells in tissues (Figure 2a,b,c,d), which is compatible with results in the literature.^[31] A circular dichroism spectrophotometer was employed in order to study the secondary structure of peptide nanofibers used in this study, which were found to have predominant β -sheet structures with a chiral absorbance maximum at around 200 nm and minimum at around 220 nm (Figure 2e). The mechanical properties of the PA gels were analyzed with oscillatory rheology. When designing a scaffold for nervous tissue, it is important to consider the mechanical characteristics of the scaffold since the brain tissue has a stiffness of about 1 kPa.^[32] Besides biological cues, mechanical properties of PA nanofibers were also considered in order to create an ECM-like environment similar to ECM of nervous tissue. The rheology results confirmed that all PA combinations had higher storage modulus (G') than loss modulus (G''), verifying the gel formation at physiological pH, formed gels and displayed similar properties to the nervous tissue (Figure 2f).

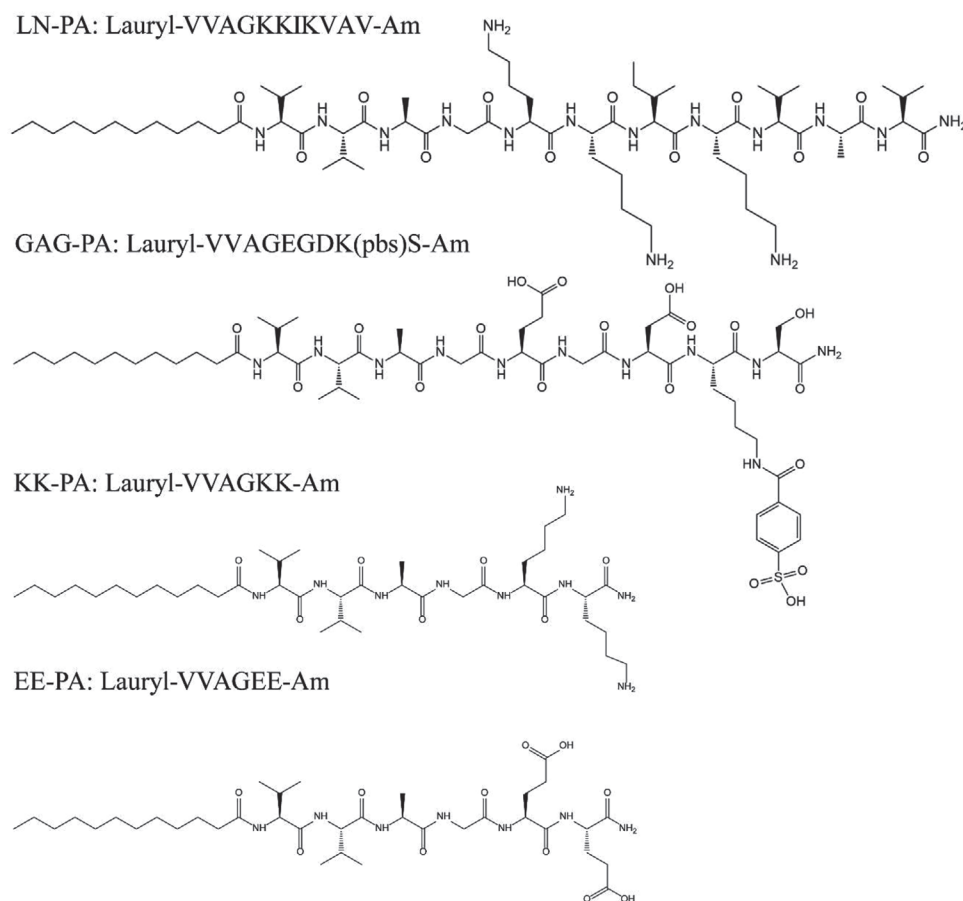


Figure 1. Chemical structures of the PA molecules used in the study.

2.2. Nanofiber Scaffolds Support the Adhesion and Neurite Extension of Isolated DRG Neurons

It is important to assess the biocompatibility and bioactivity of the manufactured scaffolds prior to *in vivo* testing. Since DRG neurons are one of the two types of neurons found in the spinal cord, the bioactivity of these scaffolds was investigated using DRG neurons. In order to achieve this, we seeded freshly isolated DRG neurons on coverslips coated with prepared nanofiber scaffolds, or poly-D-Lysine (PDL)-Laminin, which was used as a positive control. The experimental nanofiber scaffolds were as follows: GAG-mimetic scaffold KK-PA/GAG-PA, laminin-mimetic scaffold LN-PA/EE-PA, dual bioactive scaffold LN-PA/GAG-PA, and the non-bioactive control scaffold KK-PA/EE-PA. Immunostaining against β III-tubulin performed at 7 days of culture showed that the DRG neurons attached to the scaffolds in all experimental groups, and extended neurites in all groups (**Figure 3**). It was not possible to quantify the viability and adhesion of the neurons on the scaffolds, because the cell isolation protocol requires use of chemotherapeutics to kill non-neuronal cells such as Schwann cells or fibroblasts,^[33] which are seeded with DRG neurons during isolation; thus, there were loosely attached or dead non-neuronal cells in all groups. Therefore, DRG neurons were analyzed in terms of their neurite-outgrowth capacity on different PA

combinations through immunostaining of β III-tubulin. Morphology of the DRG neurons after 7 days of culture on the scaffolds suggested that these scaffolds supported the adhesion and neurite extensions of the DRG neurons *in vitro*. DRG neurons have an innate ability to regenerate; therefore, neurite extension was observed on all scaffolds. The neurite extension potential of DRG neurons on LN-PA/GAG-PA scaffold displayed a similar pattern compared to the positive control. Previously, Silva et al. showed that neurite-promoting laminin epitope IKVAV bearing nanofiber scaffold induced very rapid differentiation of cells into neurons, while discouraging the development of astrocytes.^[34] Also, our previous research showed that the double bioactive scaffold promoted neurite extension significantly better compared to laminin mimetic scaffold or GAG mimetic scaffold,^[30] we decided to include only the double bioactive scaffold for the *in vivo* studies for reducing the number of animals in the experiments.

2.3. Functional Recovery after SCI

We used the BBB locomotor scale in order to assess the functional recovery from the experimental SCI model.^[35] Horizontal incision causes partial separation in the right half of the spinal cord and does not lead to complete rupture. A single-sided

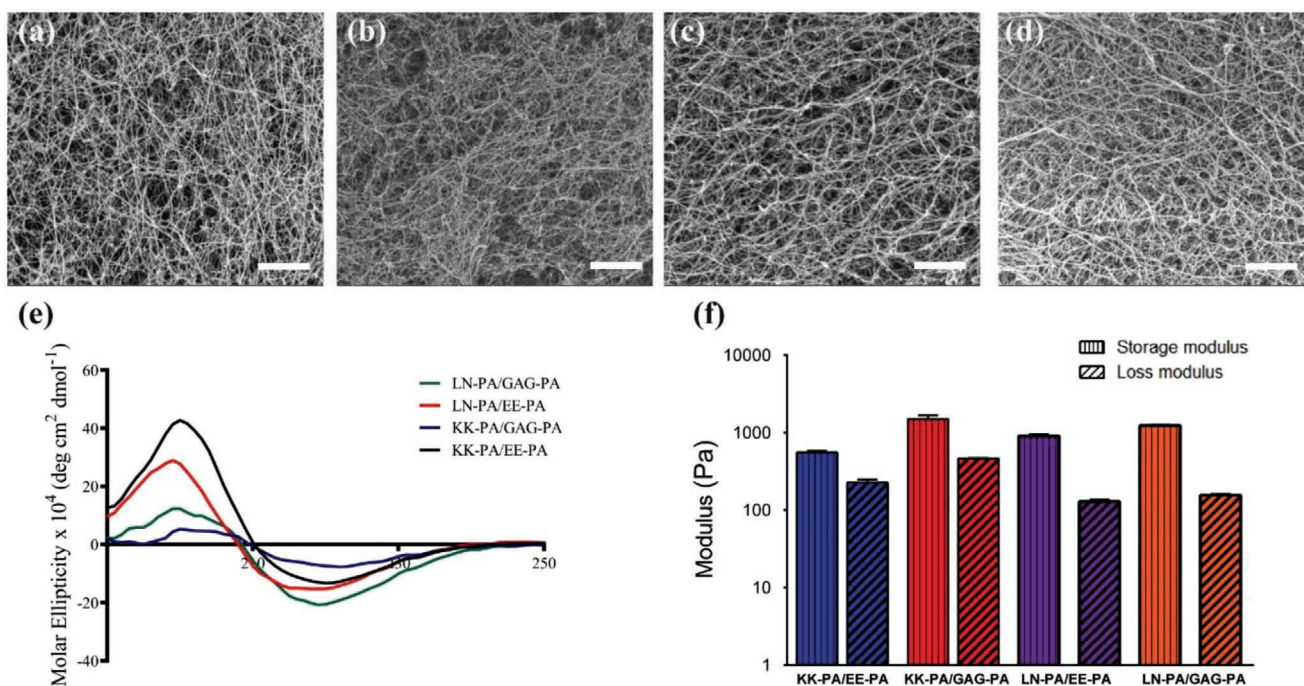


Figure 2. SEM images of KK-PA/EE-PA (a), KK-PA/GAG-PA (b), LN-PA/EE-PA (c), and LN-PA/GAG-PA (d) shows the nanofiber networks resembling the natural ECM structure. Scale bars are 1 μm in length. e) Characterization of the secondary structure of peptide nanostructures by circular dichroism. All PA combinations were found to have β-sheet secondary structure by circular dichroism analysis. f) The mechanical properties of PA gels measured by oscillatory rheology. The rheology results showed gelation as a result of nanofibrous network formation for all PA combinations at pH 7.4.

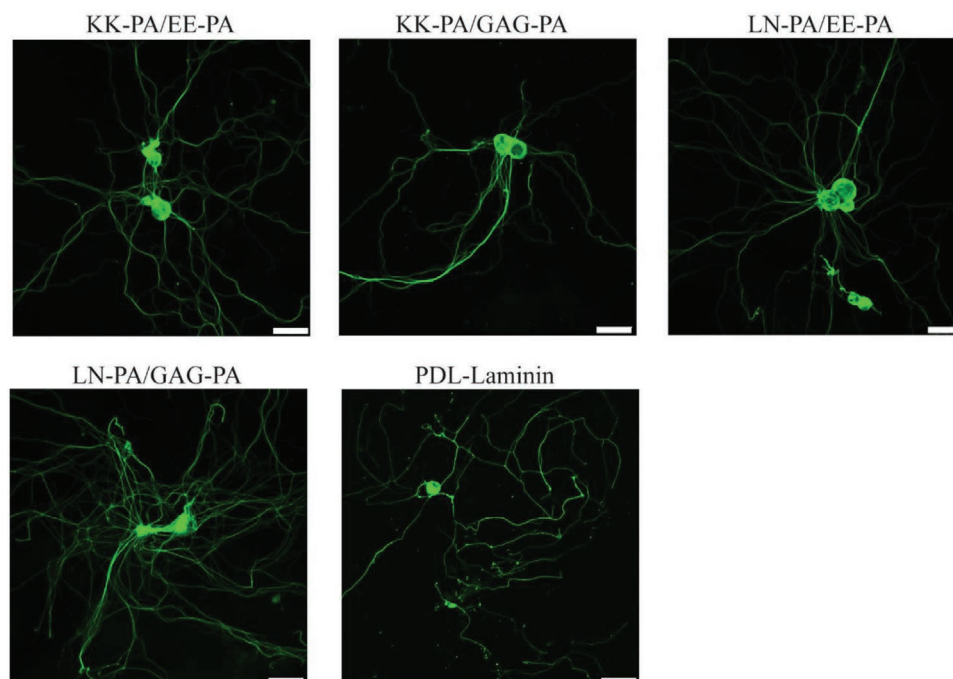


Figure 3. DRG neurons cultured on KK-PA/EE-PA, KK-PA/GAG-PA, LN-PA/EE-PA, LN-PA/GAG-PA and PDL-Laminin coated surfaces for 7 days were immunostained against βIII-tubulin (green) and were imaged by confocal microscopy. Scale bar is 50 μm. Nanofiber scaffolds supported the adhesion of the DRG neurons and neurite extension was apparent on all surfaces.

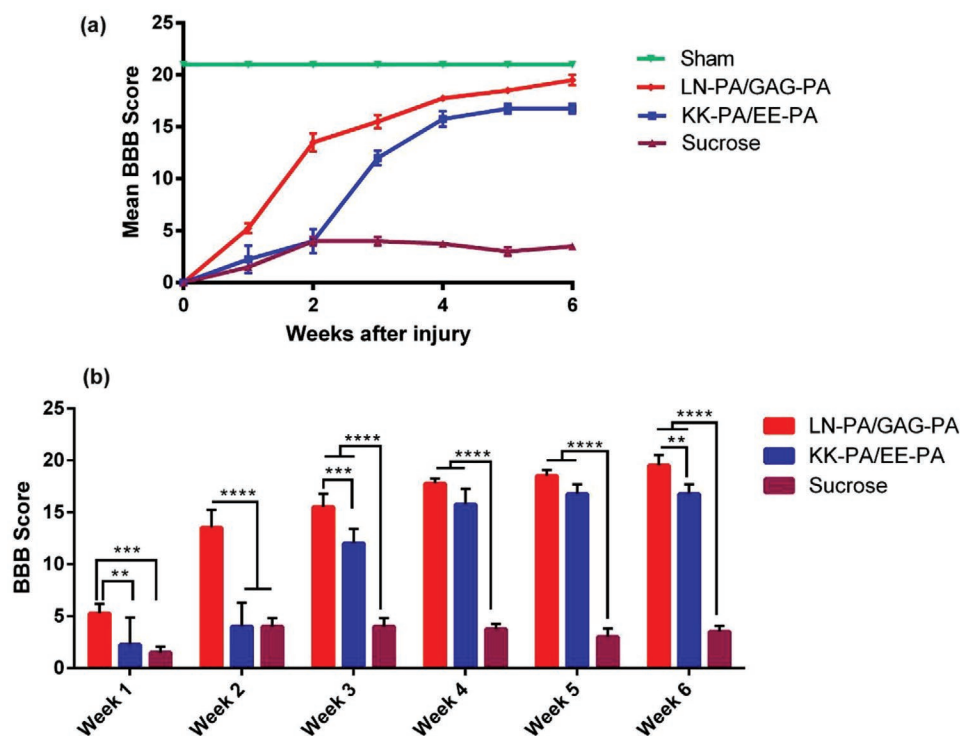


Figure 4. LN-PA/GAG-PA nanofibers promote functional recovery after SCI as analyzed by the BBB scale. a) Graph showing the time course of locomotor recovery as measured by BBB scores during 6 weeks for sham, LN-PA/GAG-PA, KK-PA/EE-PA, and sucrose treated groups (error bars represent standard deviation). (b) Bar graphs showing BBB locomotor scores after SCI. LN-PA/GAG-PA, KK-PA/EE-PA, and sucrose treated groups were analyzed with two-way ANOVA with Bonferroni post-test. Values represent mean \pm Standard deviation (SD) (**** p < 0.0001, *** p < 0.001, ** p < 0.01).

horizontal incision with the needle causes damage to the CNS, resulting in a nearly complete loss of strength in the hindlimb and paralysis. BBB scoring was based on the contribution of the hindlimb on the side of the incision to motor motion. The contribution of the left hindlimb was not evaluated for the BBB score since there was no incision on the left side of the spinal cord. For this and all subsequent experiments, the researchers were kept blind to the identity of the treatment groups of the animals. The BBB scores at each time-point are shown in **Figure 4**. As expected, the sham group achieved the highest BBB score (21 points) from the first week after the surgical intervention since their spinal cords were not injured during the surgery.

While creating spinal cord damage by using semi-incision model, the same force loss cannot be achieved in all rats even though a standard incision. While sometimes a loss of full strength is observed, for other cases there are small muscle group movements in the muscles that cannot be detected in the examination. The reason for this difference is that some motor conduction pathways in the spinal cord are still unclear. This is also another reason for evaluating the BBB score separately for each rat before and after the incision for each time point. The results after injury and injection of the bioactive PA gel (LN-PA/GAG-PA) and the non-bioactive PA gel (KK-PA/EE-PA) were compared to assess whether the effects were mediated by the bioactive peptide signals. The control PA (KK-PA/EE-PA) contained no bioactive epitope but still formed nanofibers similar to LN-PA/GAG-PA. The BBB scores of the LN-PA/GAG-PA treated group were higher than those of the sucrose and

KK-PA/EE-PA treated group, especially during the 1st, 2nd and 3rd weeks post-injury. During the 1st and 2nd week after the injury, KK-PA/EE-PA and sucrose injected groups did not differ from one another, and the animals in both groups scored less than the LN-PA/GAG-PA treated group. Although there was an increase in the scores of the KK-PA/EE-PA treated group during the following weeks, these scores were still less than the bioactive group. Strikingly, at the end of the 6th week, the mean BBB score of LN-PA/GAG-PA treated group was almost equal to those in sham group.

The injury we created does not cause a full incision. With the presence of undamaged, healthy tissue parts in the spinal cord and mechanical support provided by nanofibers, functional recovery as revealed with BBB locomotor scale was found to be better in nanofiber treatment regardless of presence of bioactivity, compared to sucrose group. There is also a recovery in non-bioactive peptide nanofiber group, potentially due to its physical properties resembling the natural ECM. However, compared to non-bioactive peptide nanofibers, early response (first 3 weeks) in BBB scores was better in bioactive peptide nanofibers since they introduce bioactive signals for cell binding, neurite extension and increase the local concentrations of growth factors.

Preparation of animal models for SCI and paralysis can be performed with many ways such as needle pricking, drop weight, complete incision of hemi-cord or superficial incision. If the damage is mild, rapid recovery occurs. In general, fractures of the spine may result in unilateral or bilateral

rupture, dissociation or only superficial damage as a result of pressure on the spinal cord by contusion or fracture due to the severity of trauma, there are also undamaged parts in the anterior region of the spinal cord. The white matter surrounding the spinal cord is usually damaged during the accidents. Even if there is no total right half incision, paralysis is observed when the white matter is damaged. The aim of this study was to observe the healing process of the white matter via bioactive peptide nanofibers without making a total incision.

Bioactive peptide nanofibers used in this study introduce bioactive epitopes, which mimic natural laminin and glycosaminoglycan molecules in the ECM of the cells. Laminin-mimetic IKVAV sequences provide cell binding and neurite extension, which increase the functional recovery after SCI. Also, heparan sulfate mimetic peptide nanofibers interact with growth factors and increase their local concentrations, which is also another possible mechanism to induce functional recovery. Overall, these experimental results showed the synergistic effects of laminin and heparan sulfate signals in the treatment of SCI and demonstrated that this dual bioactivity was able to effectively promote neural regeneration and functional recovery in rats following SCI.

2.4. Effects of the ECM Mimetic Peptide Nanofibers on Tissue Integrity and Neural Regeneration

For SCI, lateral hemisection was used in experimental groups, where only one side of the spinal cord was damaged. After the

formation of injury and PA treatment, spinal cords were dissected from the animals at the end of 6 weeks and hematoxylin and eosin (H&E) staining was carried out on spinal cord sections in order to examine the morphology. Since the cavities formed in the injured spinal cord are one of the most problematic physical obstacles for axonal regeneration, structural recovery, and gain of function, it is important to fill these cavities with a material similar to the native ECM. Histological analysis showed that the hemisection SCI model resulted in severe loss of gross tissue structure, which could be observed as alterations in the sucrose-treated group. In contrast, LN-PA/GAG-PA injection to the spinal cord provided better tissue integrity compared to sucrose and KK-PA/EE-PA treated control groups. The gel was degraded at the end of 6 weeks, and cells accumulated toward the injury site and almost covered this area (**Figure 5**; Figures S2–S5, Supporting Information). This result indicated that the bioactivity introduced by LN-PA/GAG-PA scaffold helped to maintain tissue integrity at the injury site.

β -III tubulin is a commonly used marker in neuronal differentiation and regeneration studies, since it is expressed in both mature and immature neurons.^[36,37] Immunohistochemistry staining against β III-tubulin, which plays a critical role in proper axon guidance and maintenance, showed higher expression of this protein in the bioactive group while the expression of this protein was not sustained in control groups due to the disruption of the tissue integrity (**Figure 6**; Figures S2–S5). β -III tubulin staining also showed that the cells that accumulated toward the injection site in gel in bioactive group were

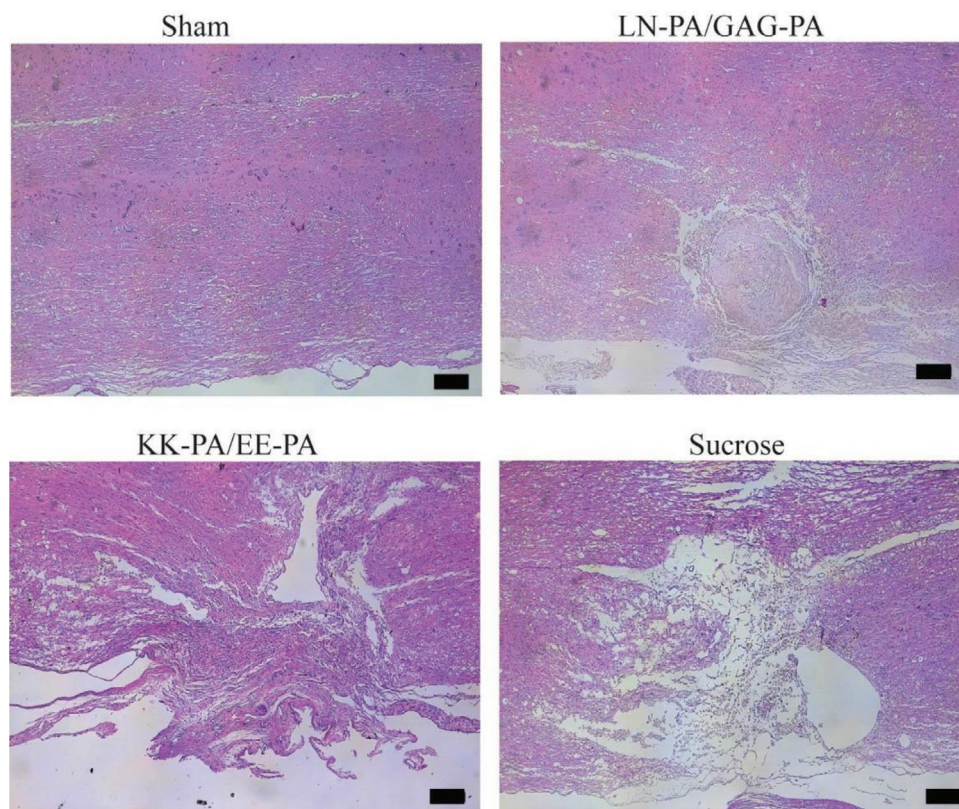


Figure 5. H&E staining of rat spinal cord sections at postoperative week 6. The sections of LN-PA/GAG-PA group were compared with that of sham, KK-PA/EE-PA, and sucrose treated groups. Images were taken at 100 \times magnification (Scale bars are 200 μ m in length).

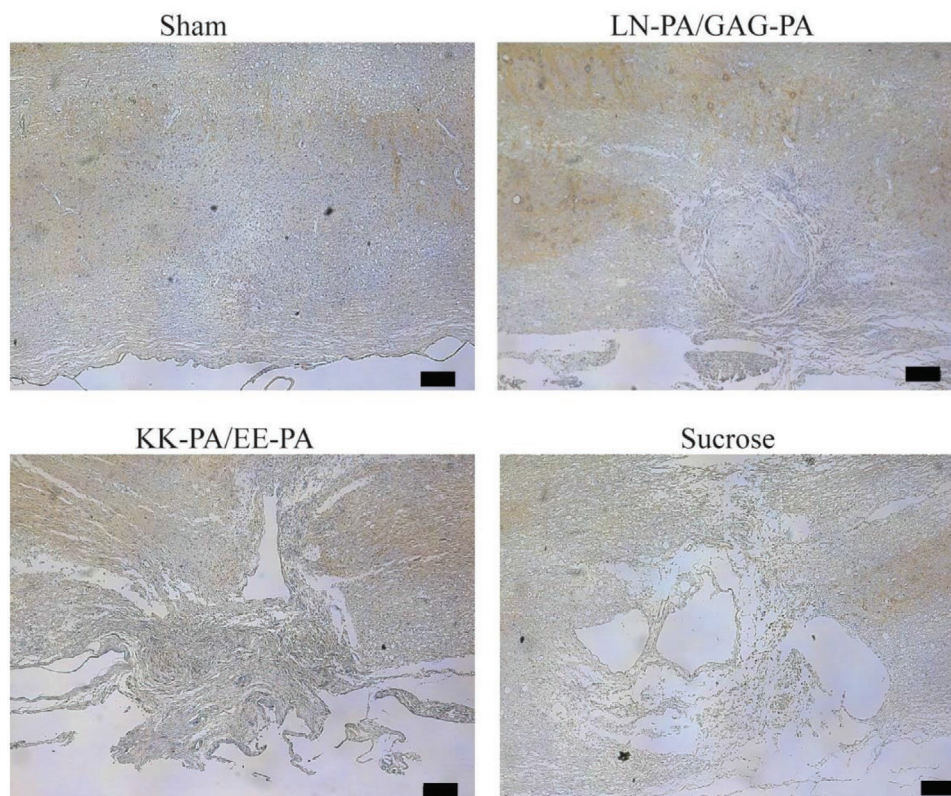


Figure 6. Immunohistochemistry against β III-tubulin protein for rat spinal cord sections at postoperative week 6. The sections of LN-PA/GAG-PA group were compared with that of sham, KK-PA/EE-PA and sucrose treated groups. Images were taken at 100 \times magnification (Scale bars are 200 μ m in length).

characterized as neurons due to positive staining against β -III tubulin. In order to track the apoptotic activity and astrocytes at the injury site, caspase III and glial fibrillary acidic protein (GFAP) staining was also performed, respectively. Immunohistochemistry results revealed that there was no caspase III or GFAP staining at the injury site in LN-PA/GAG-PA treated group as in the sham group (Figures S1–S5). Therefore, during regeneration process, the cells accumulated at the injury site in the bioactive group were characterized as neurons instead of astrocyte, and no apoptotic activity was observed as indicated with caspase staining.

3. Conclusion

Herein the bioactive laminin-GAG mimetic PA nanofiber gel system was used for therapeutic effect in both for DRG neurons in vitro and in experimental hemisection sciatic nerve injury model in vivo. In vitro results revealed that the laminin-derived peptide signals together with heparan-sulfate-mimicking epitope promoted the adhesion, viability, and neurite extension of isolated DRG neurons. Moreover, in vivo results indicated that this bioactive scaffold provided better tissue integrity and functional improvement 6 weeks after the SCI. This is the first study which combines the bioactive signals for mimicking both laminin and heparan sulfate for their regenerative effect in SCI model. This approach is beneficial in terms of the design and implantation of bioactive signals through peptide nanofiber

system with the optimal material properties such as mechanical strength, porosity, cell-adhesion and biocompatibility. Overall, these results suggest that the ECM mimetic neuroactive peptide nanofibers with dual bioactivity present a promising therapeutic material for SCI.

4. Experimental Section

Materials: All protected amino acids, lauric acid, 4-(2',4'-dimethoxyphenyl-Fmoc-aminomethyl)-phenoxyacetamidonorleucyl-4-Methylbenzhydrylamine (MBHA) resin (Rink amide MBHA resin), 2-(1H-benzotriazol-1-yl)-1,1,3,3-tetramethyluroniumhexafluorophosphate (HBTU) were purchased from NovaBiochem. Other chemicals used for peptide synthesis and material characterizations, including dichloromethane (DCM), dimethylformamide (DMF), Diisopropylethylamine (DIEA), acetonitrile, piperidine, acetic anhydride, and trifluoroacetic acid (TFA) were purchased from Sigma-Aldrich. Anti- β III tubulin, anti-caspase III, and anti-GFAP primary antibodies, all secondary antibodies, hematoxylin, eosin, BSA, Poly-D-Lysine, laminin, mounting medium, ethanol, xylene and sucrose were purchased from Sigma-Aldrich. Prolong-Gold Antifade, 3,3'-diaminobenzidine (DAB) substrate kit, TO-PRO-3 Iodide, nerve growth factor (NGF) and the materials used in cell culture studies including medium, serum, L-glutamine and penicillin-streptomycin were purchased from Thermo Scientific.

Peptide Amphiphile Synthesis and Purification: PA molecules were synthesized by using Fmoc-protected solid phase peptide synthesis method on Rink amide MBHA resin according to a previously described method.^[18,20] Briefly, the couplings of the amino acids were carried out through mixing amino acids activated with HBTU and DIEA. 20%



piperidine–dimethylformamide (DMF) solution was used for Fmoc removal. The unreacted amine groups were permanently acetylated with 10% acetic anhydride–DMF solution after coupling. DMF and DCM were used as washing solvents. *p*-Sulfobenzoic acid was coupled to the side chain of lysine to synthesize sulfonated PAs. A lysine residue with 4-methyltrityl (Mtt) side chain protection was used for selective deprotection of amine groups. Mtt removal was performed with trifluoroacetic acid (TFA): triisopropylsilane (TIS):H₂O:DCM. Cleavage of the PA molecules and the protection groups from the resin was carried out by using a mixture of TFA:TIS:H₂O. After the removal of excess TFA, PAs were precipitated with ice-cold diethyl ether, and lyophilized for further use.

Characterization and purification of the PAs was performed as previously described.^[18] Briefly, mass spectrum was obtained with Agilent LC-MS equipped with Agilent 6530 Q-TOF with an ESI source and Zorbax Extend-C18 2.1 × 50 mm column for basic conditions and Zorbax SB-C8 4.6 × 100 mm column for acidic conditions. Peptide purification was carried out with an Agilent preparative reverse-phase HPLC system equipped with a Zorbax Extend-C18 21.2 × 150 mm column for basic conditions and with a Zorbax SB-C8 21.2 × 150 mm column for acidic conditions. All peptide batches were freeze-dried and dissolved in ultrapure water before usage.

Scanning Electron Microscopy (SEM): In order to analyze the network structure of PA nanofibers, they were visualized with SEM. 30 μL of positively and negatively charged PA solutions were mixed to produce gel structures through charge neutralization. Gels were formed on silicon wafers and dehydrated with increasing ethanol concentrations. A critical point dryer (Autosamdri 815B equipment from Tousimis) was used to dehydrate the nanofibers, and the dehydrated nanofibers were coated with Au/Pd prior to examination with SEM. SEM (FEI Quanta 200 FEG) images were obtained with Everhart–Thornley Detector (ETD) at high vacuum mode at 5 keV beam energy.

Circular Dichroism (CD): Positively and negatively charged PA solutions at a concentration of 2.5×10^{-4} M were mixed to trigger the formation of nanofibers. Measurements were carried out via Jasco J815 CD spectrometer from 300 to 190 nm by adjusting data interval and data pitch to 0.1 nm and scanning speed to 100 nm min⁻¹. Digital Integration Time (DIT) was adjusted to 1 s and band width to 1 nm. All measurements were repeated 3 times.

Oscillatory Rheology: An Anton Paar Physica RM301 Rheometer, operating with a 25 mm parallel plate configuration at 25 °C, was used for the measurements. To obtain similar mechanical properties to the nervous tissue, PA molecules were used in different concentrations: (KK-PA/EE-PA (10 mM/10 mM), KK-PA/GAG-PA (6 mM/4 mM), LN-PA/EE-PA (4 mM/6 mM), and LN-PA/GAG-PA (4 mM/4 mM)). 250 μL of total PA solutions were prepared and loaded onto the lower plate center, and then gels were incubated at room temperature for 10 min before each measurement to neutralize the charge and induce gelation. After equilibrium, the upper plate was lowered to have a gap distance of 0.5 mm. Storage modulus (*G'*) and loss modulus (*G''*) values were scanned from 100 to 0.1 rad s⁻¹ of angular frequency, with a 0.5% shear strain. All measurements were repeated 3 times.

In Vitro Studies: DRG Isolation and Culture: DRG cells were isolated from 8–12 weeks old male Wistar rats according to a previously described method.^[33] Briefly, rats were sacrificed by CO₂ asphyxiation, their spinal columns were dissected and washed with ice-cold Hank's balanced salt solution (HBSS) containing 1.6 μg mL fungizone. Excess tissue around the spinal columns was trimmed, and the spinal columns were cut in half through the sagittal plane. Under a stereomicroscope, the DRGs were identified and collected in ice-cold HBSS by grasping and gently pulling up with fine forceps. The nerve trunks were trimmed using a surgical blade and HBSS was replaced with 3 mL of 0.125% solution of collagenase in DRG culture medium (F-12 medium containing 10% horse serum, 1% penicillin/streptomycin, 2 μM L-glutamine, supplemented with 50 μM 5-fluoro-2'-deoxyuridine and 150 μM uridine, 200 ng mL nerve growth factor (NGF) and 100 μg mL normocin-O). Enzymatic digestion was allowed for 2 h at 37 °C, with replacing the collagenase solution

with a fresh aliquot at 1-h mark. At the end of the digestion, the DRGs were collected in a sterile falcon tube with 3 mg of Deoxyribonuclease 1 (DNase1) and centrifuged at 500 g for 1 min. The resulting DRG pellet was resuspended in 1.5 mL of DRG culture medium and cells were mechanically dissociated by pipetting until a homogenous suspension was obtained. The suspension was filtered through a 100 μm cell strainer and the filtrate was evenly distributed on the peptide nanofiber, or PDL-Laminin coated coverslips. The DRG neuron culture was allowed for 7 days in a 37 °C humidified chamber with 3% CO₂ atmosphere, while refreshing the cell medium at days 3 and 5. At the end of 7 days, DRG cells were fixed with 4% paraformaldehyde for immunocytochemistry.

In Vitro Studies: Immunocytochemistry of DRG Cells: DRG neurons were cultured on peptide nanofibers for 7 days, fixed in 4% paraformaldehyde prepared in phosphate buffered saline (PBS) for 20 min, permeabilized with 0.1% (v/v) Triton-X-100 in PBS for 20 min, and blocked with a solution of 5% (w/v) bovine serum albumin (BSA) in PBS containing 10% normal goat serum for 2 h. Then, the cells were incubated with anti-βIII tubulin primary antibody (Abcam; ab78078) diluted according to the manufacturer's recommendation in 1% BSA in PBS, overnight at 4 °C. The next day, the primary antibody solution was removed, cells were washed in PBS, and incubated for 1 h at room temperature with goat-anti-mouse secondary antibody conjugated with Cy2. Cells were then counterstained with 1 μM TO-PRO-3 iodide in PBS for 15 min. Samples were washed and mounted with ProLong Gold Antifade reagent and imaged with a Zeiss LSM 510 inverted confocal microscope.

In Vivo Studies: Animals: Male Wistar rats (weighing 300–350 g) were housed individually with free access to food and water in a 12 h/12 h light/dark cycle. Experimental procedures conformed to the National Institute of Health Guide for the Care and Use of Laboratory Animals and were approved by the Local Ethics Committee on Experimental Animal Research of Ankara University, Ankara, Turkey (Approval ID: 2015-16-183).

In Vivo Studies: Rat SCI, PA Injection, and Animal Care: Animals were deeply anesthetized by an intraperitoneal injection of ketamine and xylazine. For the surgery of each rat, the rat's back was shaved, and a skin incision was made along the midline of the back. The laminae were exposed, and a laminectomy was performed at the level of T9 or T10. The midline of the spinal cord was identified, and a transverse cut was made laterally from midline to create a hemisection injury. After injury, a total of 10 μL of 1% LN-PA (5 μL) and 1% GAG-PA (5 μL) were mixed and injected using a 1–10 μL pipette into the injury site. 1% KK-PA (5 μL) and 1% EE-PA (5 μL) were also mixed in order to form the gel, and this gel was injected as an epitope-free control group. Sucrose solution was injected to a group of rats with SCI in order to serve as the negative control. Another group of rats underwent the same operation without SCI and injection in order to serve as the sham control.

In Vivo Studies: Behavioral Analyses: The BBB scale is a semiquantitative scale based on the locomotor response of rats that can take values ranging from zero to 21.^[35] Neurobehavioral analysis was performed using the BBB scale, and was evaluated at the end of each week. Hind limb paralysis was scored as 0 points, while a completely normal spinal cord was scored as 21 points. The spinal cord functions were scored according to the number and motion range. The assessment was performed by two physicians independently, using a double-blind method, and the average values of the two test results were taken as the recording values.

In Vivo Studies: Animal perfusions and tissue acquisition: Six weeks after the peptide nanofiber injection, rats in all groups were sacrificed with transcardiac perfusion for further histological studies using 4% paraformaldehyde solution in PBS under ketamine and xylazine anesthesia. The spinal cords were dissected and fixed in 4% paraformaldehyde solution. The spinal cords obtained following perfusion were further sectioned and processed for immunohistochemical analyses.

In vivo Studies: Immunohistochemistry: Sections were deparaffinized in xylene and rehydrated in serial ethanol series for H&E staining according to the standard protocol. For immunohistochemistry experiments, sections were stained with anti-βIII tubulin (1:100, Millipore), anti-GFAP

(1:200; Millipore) and anti-caspase III (1:2000, Cell Signaling Technology) antibodies. After primary antibody staining, horseradish peroxidase conjugated goat anti-rabbit or goat anti-mouse secondary antibodies (1:500; Millipore) was used. In order to generate a brown precipitate on specific antibody locations, 3,3'-diaminobenzidine (DAB) staining was performed. Xylene based mounting medium was used to mount the samples on slides. Digital images were acquired via Zeiss Axio Scope A1 by using 10x and 20x objectives.

Statistical Analysis: All quantitative values are presented as mean \pm standard error of means (sem), and experiments were performed with at least three replicates. One-way ANOVA was used for statistical analyses, and a p-value of less than 0.05 was considered as statistically significant.

Supporting Information

Supporting Information is available from the Wiley Online Library or from the author.

Acknowledgements

The authors thank Ms. Z. Erdogan and Mr. M. Guler for their technical help in purification and characterization methods. M.S. was supported by TUBITAK-BIDEB (2211) Ph.D. fellowship. A.B.T. acknowledges support from the Science Academy Outstanding Young Scientist Award (BAGEP).

Conflict of Interest

The authors declare no conflict of interest.

Keywords

extracellular matrix, glycosaminoglycan, laminin, peptide nanofibers, spinal cord regeneration

Received: July 8, 2020

Revised: September 23, 2020

Published online: October 11, 2020

-
- [1] C. E. Hulsebosch, *Adv. Physiol. Educ.* **2002**, *26*, 238.
 [2] M. E. Schwab, D. Bartholdi, *Physiol. Rev.* **1996**, *76*, 319.
 [3] A. M. Avellino, D. Hart, A. T. Dailey, M. MacKinnon, D. Ellegala, M. Kliot, *Exp. Neurol.* **1995**, *136*, 183.
 [4] M. B. Bracken, M. J. Shepard, W. F. Collins, T. R. Holford, W. Young, D. S. Baskin, H. M. Eisenberg, E. Flamm, L. Leo-Summers, J. Maroon, L. F. Marshall, P. L. Perot Jr., J. Piepmeier, V. K. H. Sonntag, F. C. Wagner, J. E. Wilberger, H. R. Winn, *N. Engl. J. Med.* **1990**, *322*, 1405.
 [5] P. J. Reier, B. T. Stokes, F. J. Thompson, D. K. Anderson, *Exp. Neurol.* **1992**, *115*, 177.
 [6] M. Oudega, X. M. Xu, *J. Neurotrauma*. **2006**, *23*, 453.
 [7] S. David, A. J. Aguayo, *Science* **1981**, *214*, 931.
 [8] J. W. McDonald, X. Z. Liu, Y. Qu, S. Liu, S. K. Mickey, D. Turetsky, D. I. Gottlieb, D. W. Choi, *Nat. Med.* **1999**, *5*, 1410.
 [9] C. P. Hofstetter, E. J. Schwarz, D. Hess, J. Widenfalk, A. El Manira, D. J. Prockop, L. Olson, *Proc. Natl. Acad. Sci. U S A* **2002**, *99*, 2199.
 [10] S. Karimi-Abdolrezaee, E. Eftekharpour, J. Wang, C. M. Morshead, M. G. Fehlings, *J. Neurosci.* **2006**, *26*, 3377.
 [11] J. S. Guo, Y. S. Zeng, H. B. Li, W. L. Huang, R. Y. Liu, X. B. Li, Y. Ding, L. Z. Wu, D. Z. Cai, *Spinal Cord* **2007**, *45*, 15.
 [12] T. Mitsui, I. Fischer, J. S. Shumsky, M. Murray, *Exp. Neurol.* **2005**, *194*, 410.
 [13] H. M. Geller, J. W. Fawcett, *Exp. Neurol.* **2002**, *174*, 125.
 [14] C. E. Schmidt, J. B. Leach, *Annu. Rev. Biomed. Eng.* **2003**, *5*, 293.
 [15] M. R. Scott, R. Will, J. Ironside, H. O. Nguyen, P. Tremblay, S. J. DeArmond, S. B. Prusiner, *Proc. Natl. Acad. Sci. U S A* **1999**, *96*, 15137.
 [16] M. J. Moore, J. A. Friedman, E. B. Lewellyn, S. M. Mantila, A. J. Krych, S. Ameenuddin, A. M. Knight, L. Lu, B. L. Currier, R. J. Spinner, R. W. Marsh, A. J. Windebank, M. J. Yaszemski, *Biomaterials* **2006**, *27*, 419.
 [17] H. Nomura, C. H. Tator, M. S. Shoichet, *J. Neurotrauma* **2006**, *23*, 496.
 [18] G. Gunay, M. Sever, A. B. Tekinay, M. O. Guler, *Biotechnol. J.* **2017**, *12*, 1700080.
 [19] M. Sever, G. Gunay, M. O. Guler, A. B. Tekinay, *Biomater. Sci.* **2018**, *6*, 1859.
 [20] M. Sever, M. Turkyilmaz, C. Sevinc, A. Cakir, B. Ocalan, M. Cansev, M. O. Guler, A. B. Tekinay, *Acta Biomater.* **2016**, *46*, 79.
 [21] V. M. Tysseling, V. Sahni, E. T. Pashuck, D. Birch, A. Hebert, C. Czeisler, S. I. Stupp, J. A. Kessler, *J. Neurosci. Res.* **2010**, *88*, 3161.
 [22] V. M. Tysseling-Mattiace, V. Sahni, K. L. Niece, D. Birch, C. Czeisler, M. G. Fehlings, S. I. Stupp, J. A. Kessler, *J. Neurosci.* **2008**, *28*, 3814.
 [23] J. D. Hartgerink, E. Beniash, S. I. Stupp, *Science* **2001**, *294*, 1684.
 [24] H. Cui, M. J. Webber, S. I. Stupp, *Biopolymers* **2010**, *94*, 1.
 [25] K. Tashiro, G. C. Sephel, B. Weeks, M. Sasaki, G. R. Martin, H. K. Kleinman, Y. Yamada, *J. Biol. Chem.* **1989**, *264*, 16174.
 [26] M. Durbeej, *Cell Tissue Res.* **2010**, *339*, 259.
 [27] N. J. Gardiner, *Dev. Neurobiol.* **2011**, *71*, 1054.
 [28] R. J. Riopelle, K. E. Dow, *Brain Res.* **1990**, *525*, 92.
 [29] K. Forsten-Williams, C. L. Chu, M. Fannon, J. A. Buczek-Thomas, M. A. Nugent, *Ann. Biomed. Eng.* **2008**, *36*, 2134.
 [30] B. Mammadov, R. Mammadov, M. O. Guler, A. B. Tekinay, *Acta Biomater.* **2012**, *8*, 2077.
 [31] G. Uzunalli, R. Mammadov, F. Yesildal, D. Alhan, S. Ozturk, T. Ozgurtas, M. O. Guler, A. B. Tekinay, *ACS Biomater. Sci. Eng.* **2017**, *3*, 1296.
 [32] P. C. Georges, W. J. Miller, D. F. Meaney, E. S. Sawyer, P. A. Janmey, *Biophys. J.* **2006**, *90*, 3012.
 [33] T. H. Burkey, C. M. Hingtgen, M. R. Vasko, *Methods. Mol. Med.* **2004**, *99*, 189.
 [34] G. A. Silva, C. Czeisler, K. L. Niece, E. Beniash, D. A. Harrington, J. A. Kessler, S. I. Stupp, *Science* **2004**, *303*, 1352.
 [35] D. M. Basso, M. S. Beattie, J. C. Bresnahan, *J. Neurotrauma*. **1995**, *12*, 1.
 [36] M. K. Lee, J. B. Tuttle, L. I. Rebhun, D. W. Cleveland, A. Frankfurter, *Cell Motil. Cytoskeleton* **1990**, *17*, 118.
 [37] J. R. Menezes, M. B. Luskin, *J. Neurosci.* **1994**, *14*, 5399.